Journal of Materials Chemistry C

Accepted Manuscript

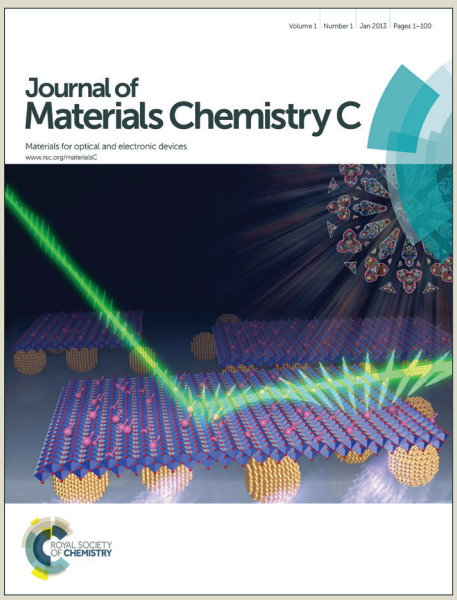

ROYAL SOCIETY OF CHEMISTRY

www.rsc.org/materialsC

Journal of Materials Chemistry C

Dynamic Article Links ►

Cite this: DOI: 10.1039/c0xx00000x

PAPER

www.rsc.org/xxxxxx

Colloidal solutions of niobium trisulfide and niobium triselenide

Vladimir E. Fedorov,*[a, b] Sofya B. Artemkina,[a, b] Ekaterina D. Grayfer,[a] Nikolay G. Naumov,[a,b] Yuri V. Mironov,[a] Alexander I. Bulavchenko,[a] Vladimir I. Zaikovskii,[b] Irina V. Antonova,[c] Alexander I. Komonov,[c] and Maxim V. Medvedev[d]

Received (in XXX, XXX) Xth XXXXXXXXX 20XX, Accepted Xth XXXXXXXXX 20XX

DOI: 10.1039/b000000x

Exfoliated nanomaterials, such as graphene and related few-layered materials, are now widely studied for electronics, electrodes and composites, so it is desirable to demonstrate exfoliation of a wider number of layered materials. We have shown that bulk niobium trichalcogenides NbS_3 and $NbSe_3$ may be stably dispersed in a number of common organic solvents by ultrasonic treatment. The most concentrated dispersions are obtained in alcoholic media (up to ~ 0.443 $g \cdot L^{-1}$). The colloids contain thin well-crystallized nanoribbons of NbS_3 and $NbSe_3$. Filtration or spraying of the colloids produces strongly textured thin films with good conducting properties.

Introduction

The 2000s saw a revived interest in layered materials and their exfoliation to nanosheets and nanoribbons by various methods. After the discovery of intriguing properties of graphene mechanically exfoliated from bulk graphite, its inorganic counterparts were also studied extensively.[1-17] Families of layered materials suitable for exfoliation are graphite, *h*-BN, metal dichalcogenides, transition metal trichalcogenides, metal halides and oxides, clays, layered double hydroxides, ternary transition metal carbides and nitrides.[7, 8] It is important to demonstrate exfoliation of a wide selection of materials.

Transition metal trichalcogenides MQ_3 (M = Ti, Zr, Hf, Nb, Ta; Q = S, Se) attracted much attention in the physics community due to their unusual properties including superconductivity, Peierls instability, charge density wave transport.[18, 19] They were also studied as lubricants[20] and as electrode materials in lithium electrochemical cell.[21, 22] Recently MQ_3 micro- and nano-structures of various morphologies have been synthesized: 2-D nanocrystals of $ZrSe_3$ and $HfSe_3$;[23] nanowires, nanoribbons and nanobelts of $NbSe_3$,[24-27] TaS_3,[28] ZrS_3,[29] HfS_3,[29] and TiS_3;[30] ring-like structures of $NbSe_3$[31] and $TaSe_3$[32]; Mobius strips of $TaSe_3$,[32, 33] $NbSe_3$, and TaS_3, and more complex morphologies.[33] DFT calculations have been made for NbS_3 nanostructures.[34] Many of these anisotropic nanostructures are achieved by carefully adjusting synthetic conditions of the vapor transport process, i.e. by bottom-up approach (from elements) as MQ_3 grow as needle- or fiber-like crystals.

In MQ_3 each metal atom is located at the center of a trigonal prism of chalcogen atoms arranged in chains along the *b* axis (Fig. 1 a, c). M-Q bond length inside the MQ_6 prisms is almost identical with M-Q bond length linking adjacent chains. Thus, strong covalent bonds are realized both inside the MQ_6 prisms and between the neighboring prisms. It means that the chains are connected in layers which face each other with Q atoms and are bonded by relatively weak Van der Waals forces (Fig. 1 b, d). Therefore, trichalcogenides may also be regarded as layered materials. Two-dimensional or layer-type character of these MQ_3 systems was proved by Raman and IR data, combined with a valence force model of the lattice dynamics[35, 36] and by experimentally observed quadratic temperature behavior of the heat capacity.[37] Therefore, MQ_3 structures may have the properties both of quasi-1D systems and layer-type (2D) structures.

Although MQ_3 are described by the same formulae, they have essential distinctions in crystal structures and electronic properties.[18] According to structural and spectroscopic data, the MQ_3 phases can be described by an ionic model $M^{4+}(Q_2)^{2-}Q^{2-}$ containing two non-equivalent states of chalcogens – simple chalcogenide ions Q^{2-} and dichalcogenide groups $(Q_2)^{2-}$. Dichalcogenide groups $(Q_2)^{2-}$ are regarded as electron reservoirs providing MQ_3 phases with some remarkable electronic properties. Triclinic NbS_3 is a semiconductor as a result of Nb–Nb (d^1–d^1) pairing in each chain (Fig. 1 a).[38-40] Monoclinic $NbSe_3$ consists of three equidistant metal chains with different $(Se_2)^{2-}$ groups (Fig.1 c); its metallic conductivity is characterized by two gigantic anomalies, at T_1 = 145K and T_2 = 59K due to the generation of two independent charge density waves in two different types of chains.[41, 42]

Two important consequences of MQ_3 structure are significant anisotropy of physical properties, as mentioned above, and ability for intercalation. Intercalation compounds with lithium,[18, 21, 22, 48] sodium[49] and hydrazine[50] are described. Ternary phases of the type Li_xMQ_3 are formed by electrochemical method or upon interaction with *n*-butyllithium. These intercalation compounds retain chain structure with relatively small expansion.[48] For

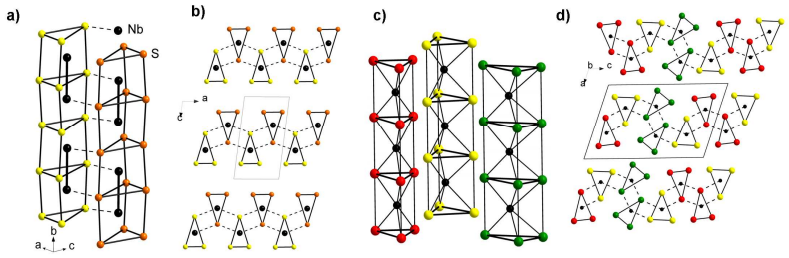

Fig. 1. Structures of trichalcogenides NbQ_3: the chains of coupled trigonal prisms [$NbQ_{6/2}$] in NbS_3 (a) and in $NbSe_3$ (b) structures along *b* axis; structure projections on the *ac* plane for NbS_3 (c) and $NbSe_3$ (d). Different sorts of prismatic columns are marked with two- and three-colour schemes.

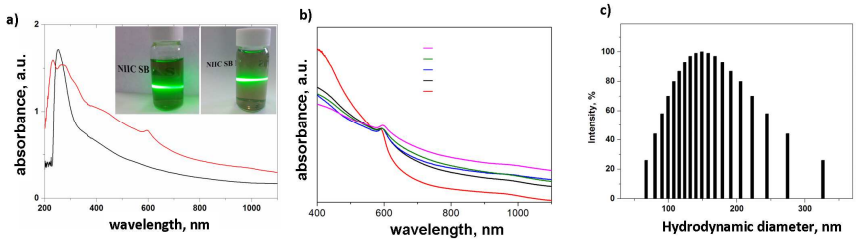

Fig. 2. Characteristics of colloidal dispersions: a) UV-*vis* spectra of the NbS_3 (red line) and $NbSe_3$ (black line) colloid solutions in acetonitrile. Inset shows Tyndall effect for NbS_3/DMF (left) and $NbSe_3$/CH_3CN (right); b) UV-*vis* spectra for NbS_3 dispersed in CH_3CN (magenta), NMP (blue), DMF (green), ^{i}PrOH (black), vol. 50% EtOH in water (red). The colloid solutions in CH_3CN, DMF, ^{i}PrOH, vol. 50% EtOH are diluted in order to bring together the absorbance bands near 600 nm for comparison; c) DLS monomodal distribution of hydrodynamic diameters for the NbS_3 dispersion in CH_3CN.

$NbSe_3$ intercalation is reversible.[21] Onuki et al. observed some exfoliation of ZrS_3 and, more significant, of $TaSe_3$ studied as cathode materials in electrochemical cells.[22] These early findings imply that MQ_3 may be exfoliated under some conditions.

Nowadays chemical exfoliation techniques widely applied to various layered materials include intercalation, oxidation and ultrasonic treatment in solvents, surfactants or polymers. Few studies mention top-down approach to the synthesis of MQ_3 nanostructures, such as exfoliation of $NbSe_3$ in surfactant solutions,[20, 25] in pyridine[27] and in toluene.[51] For example, sonication of bulk $NbSe_3$ in pyridine led to the formation of $NbSe_3$ nanowires 30 nm to 300 nm in width and 2 to 20 μm in lengths. However, these treatments produced suspensions, rather than stable colloids. If exfoliated in a liquid phase, MQ_3 could be transformed into thin films, inserted into polymers or mixed with other nanomaterials to yield interesting composites as it was done with graphene and transition metal dichalcogenides.[52] However, MQ_3, especially in a nanosized state, still remain largely unexplored materials. Therefore, since niobium trichalcogenides NbS_3 and $NbSe_3$ possess attractive physical properties and layered structure, it is the aim of this work to study liquid-phase dispersion of bulk NbS_3 and $NbSe_3$ in organic solvents and their assembly into thin films.

Results and discussion

NbS_3 and $NbSe_3$ colloidal solutions

Powdered bulk samples of triclinic NbS_3 and monoclinic $NbSe_3$ were sonicated in a number of common organic solvents. Earlier studies on carbon nanotubes, graphene, *h*-BN and MQ_2 have shown that successful exfoliation depends on the minimization of the enthalpy of mixing, which is achieved when surface energies of a dispersible material and solvent match. Coleman et al. suggest that the value of surface energy of ~70 $mJ \cdot m^{-2}$ is probably appropriate not only for carbon nanotubes and graphene but also for many Van der Waals bonded surfaces.[1] To the best of our knowledge no reports of measured surface energies of NbS_3 or $NbSe_3$ exist. Therefore we have chosen solvents which are widely available and suitable for exfoliation of carbon nanotubes, graphene and transition metal dichalcogenides (Table 1).

Table 1. Concentrations of NbS_3 and $NbSe_3$ dispersed in common solvents. The data are obtained by weighting method and are averaged from not less than five trials each.

Solvent	NbS_3 concentration in the colloid solutions ($g \cdot L^{-1}$; M)	$NbSe_3$ concentration in the colloid solutions ($g \cdot L^{-1}$; M)
DMF	0.0589; $3.11 \cdot 10^{-4}$	No dispersion
Acetone	No dispersion	No dispersion
Acetonitrile	0.191; $1.01 \cdot 10^{-3}$	0.402; $1.22 \cdot 10^{-3}$
Water	No dispersion	No dispersion
EtOH	No dispersion	0.145; $4.40 \cdot 10^{-4}$
H_2O/EtOH (1/1 vol.%)	0.443; $2.34 \cdot 10^{-3}$	No dispersion
Isopropanol	0.332; $1.76 \cdot 10^{-3}$	0.119; $3.61 \cdot 10^{-4}$
NMP	Unstable dispersion	No dispersion

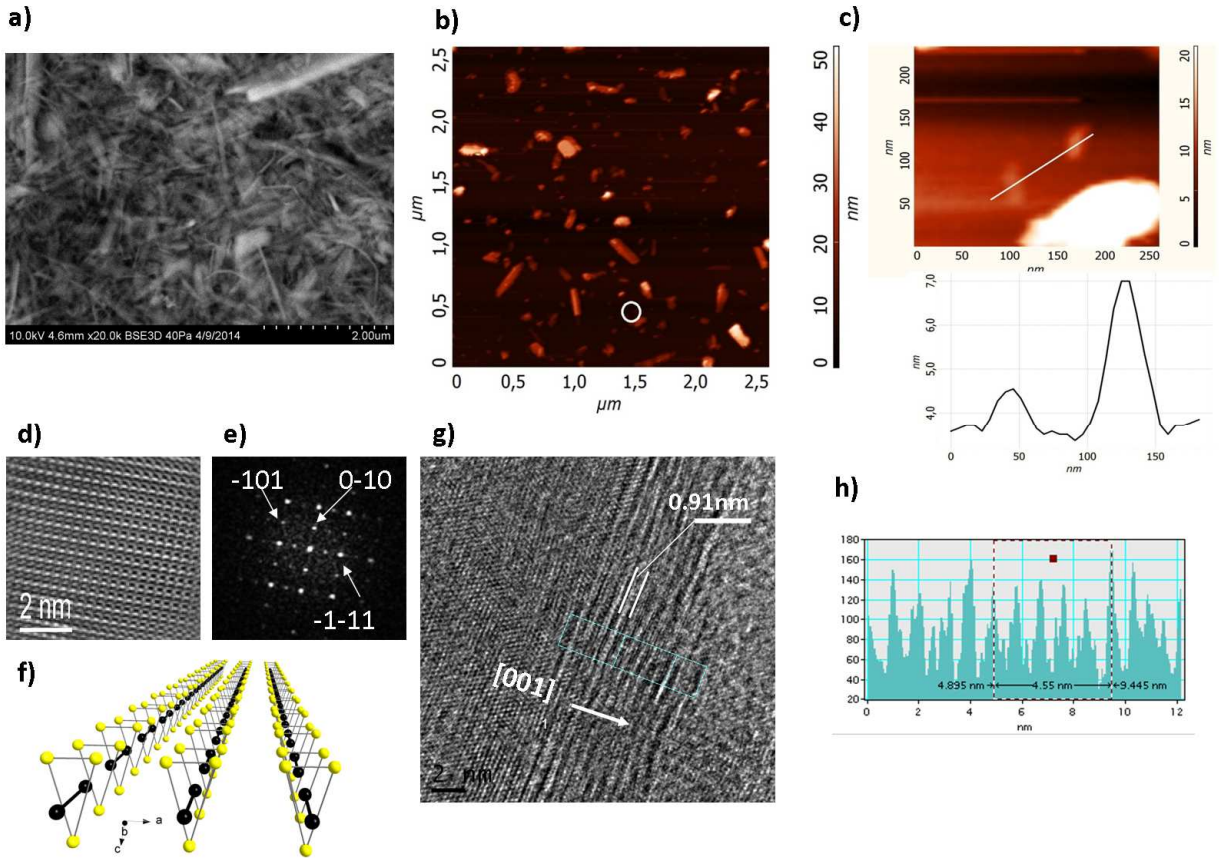

Fig. 3. Microscopy images of NbS_3 particles deposited from colloidal solution in acetonitrile: a) SEM image of NbS_3 nanoparticles filtered from colloid; b) survey AFM image of NbS_3 nanoribbons; c) AFM images of thin nanoribbons in the sample with thickness profile; d) HRTEM-image of the NbS_3 lattice indicating well-crystalline structure; e) Fourier-picture with indexed reflections; f) view of one layer of the wedge-shaped column along crystallographic direction *b* as seen in Fig. 3 d; g) HRTEM-image of a folded (001) layers of a particle with *d*-spacing 0.91 nm corresponding to *c* parameter; h) intensity profile along [001] direction for the image in Fig. 3 g.

Sonication followed by centrifugation produced stable beige-to-brown (NbS_3) or grey-pink ($NbSe_3$) transparent dispersions demonstrating Tyndall effect (light scattering on particles in the solutions) (Fig. 2 a, inset). NbS_3 and $NbSe_3$ concentrations were determined (i) by filtering the dispersions and weighing the filtered mass, and (ii) by analyzing Uv-*vis* spectra. Uv-*vis* spectra of $NbSe_3$ colloid solutions possess one band in the region near 250 nm whereas NbS_3 colloids demonstrate at least three bands in their spectra (Fig. 2 a). UV-*vis* spectra of NbS_3 dispersed in various solvents clearly show a band at 580-600 nm, the band location being slightly different from solvent to solvent (Fig. 2 b). This characteristic band can be used for determination of NbS_3 concentration in the colloid solutions. For NbS_3 colloids in CH_3CN and DMF the correlation dependences were plotted down (ESI, Fig. S1). Calculated concentrations derived from both methods are in good agreement.

In contrast to carbon nanotubes, graphene and transition metal dichalcogenides well-dispersible in high-boiling point *N*-methyl-2-pyrrolidone (NMP), our bulk NbS_3 and $NbSe_3$ showed best dispersibilities in volatile solvents, and almost no dispersibility in NMP. For $NbSe_3$ the highest concentration was found in acetonitrile (0.402 $g \cdot L^{-1}$). For NbS_3 highest concentrations of 0.332 $g \cdot L^{-1}$ and 0.443 $g \cdot L^{-1}$ were observed in isopropanol and ethanol-water mixture, respectively. EtOH/water mixture was earlier shown to exfoliate MoS_2, WS_2 and *h*-BN better than a corresponding single solvent (water or ethanol),[53] and our results confirm this finding for the case of NbS_3.

Dynamic light scattering (DLS) measurements yielded an average effective hydrodynamic diameter of ~168 nm for a NbS_3/DMF, 115 nm for $NbSe_3$/iPrOH, 153 nm for $NbSe_3$/CH_3CN, and 202 nm for $NbSe_3$/EtOH (Fig. 2 c and Fig. S2, S3 in the ESI). Microscopy studies were undertaken to further evaluate morphology, size distribution and structure of the dispersed niobium trichalcogenides. Scanning electron microscopy (SEM) images of NbS_3 filtered from colloidal solution typically contained ribbon-like particles with lengths of a few hundred nanometers and widths well below 100 nm (Fig. 3 a and Fig. S4 in the ESI). Trichalcogenide nanocrystals are elongated in the direction of *b* axis.[24, 30] AFM measurements also indicated that the particles in dispersion existed in a form of thin nanostructures with high aspect ratio which may be termed as nanoribbons. The lengths of NbS_3 nanoribbons deposited from acetonitrile dispersion were ~ 50 – 200 nm, which agrees reasonably well with DLS data taking into account that DLS characterizes a sphere that diffuses at the same rate as the solvated nanoribbon in solution (Fig. 3 b, c and Figs. S5, S6 in the ESI). The thickness of the ribbons in Fig. 3 b, c ranged approximately from 1 ~ 4 to 20 nm. For $NbSe_3$ nanoribbons

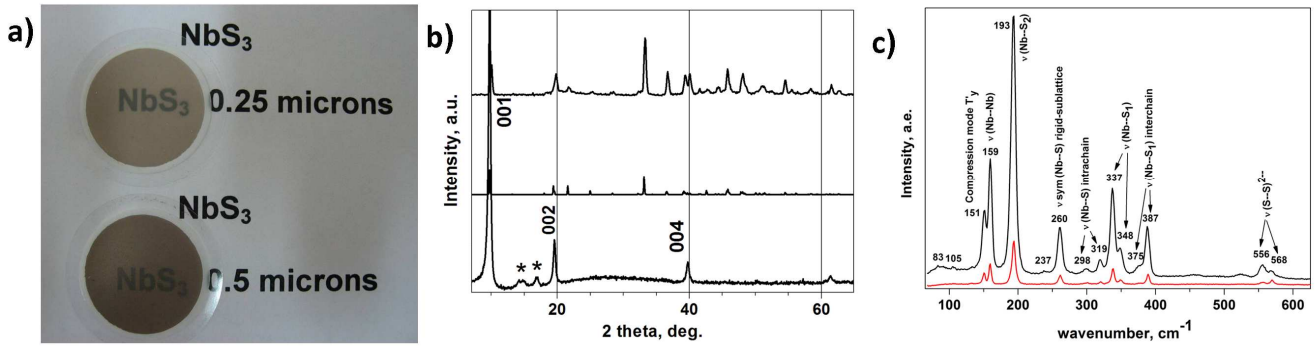

Fig. 4. Characteristics of NbS_3 films obtained via filtration through the Whatman© Anodisc membrane: a) photos of two NbS_3 films of different thickness on the membrane; b) X-ray powder diffraction patterns from powder sample prepared in high-temperature synthesis (top) and film deposited from NbS_3 colloidal dispersion in DMF (bottom); middle curve is simulated from triclinic NbS_3 structure data; c) Raman spectra of NbS_3 polycrystalline powder (bottom) and NbS_3 film (top).

deposited from the acetonitrile dispersion lengths were in the interval of ~ 50 – 400 nm, and thicknesses from ~ 3 – 40 nm (Fig. S5 in the ESI). High-resolution TEM (HRTEM) images and associated Fourier transforms (Fig. 3 d, e and Fig. S7 in the ESI) proved that the particles in dispersions retained good crystallinity with triclinic NbS_3 cell undamaged during sonication process. Lattice fringe spacings indicated in a TEM image and its Fourier transform (Fig. 3 e) were measured to be 0.672 nm, 0.457 nm, and 0.379 nm and were indexed as (010), (-101), and (-1-11) reflections of a triclinic NbS_3 particle. Fig. 3 f schematically shows packing of the prisms forming the sample surface depicted in Fig. 3 d. An example of a folded edge of NbS_3 nanoparticle is given in Fig. 3 g. Intensity profile for 5 interlayer spacings (Fig. 3 h) allows to identify the distance between these layers as 0.91 nm confirming that this is the side view of the *ab* planes. This value agrees well with the reported *c* parameter of 0.9144(4) nm.[39] The particle in Fig. 3 g contains approximately 10 – 12 double prism layers.

The question arises as to exactly how the bulk is transformed into colloid. Theoretically, there are 3 possible directions to break a trichalcogenide nanocrystal: (i) parallel to the *ab* plane (001 direction), thus exfoliating of layers from the bulk; (i) parallel to *bc* plane (100 direction), thus breaking interchain bonds; and (iii) parallel to *ac* plane, thus cutting the chain lengths. The presence of thin nanoribbons in our colloids proves that there should be exfoliation parallel to *ab* plane, as one would expect from the fact that it only requires to overcome weak Van der Waals bonds between layers. Dispersion of NbS_3 and $NbSe_3$ probably occurs in the result of solvent intercalation in the inter-prism spaces leading to delamination of the materials and stabilization of the formed colloids by the solvent molecules with appropriate surface energies. In that case, given that the thickness of a NbS_3 monolayer exfoliated along the crystallographic direction *c* is about 1 nm (1.5 nm for $NbSe_3$), this suggests that the thinnest NbS_3 nanoribbons in Fig. 3 b,c consist of 1 – 4 layers, although thicker particles are also present (the thinnest $NbSe_3$ nanoribbons consist of 2 layers and the thicker ones are up to 27 layers). Overall, microscopic characterization shows that trichalcogenide nanoribbons in colloids are thinner and shorter than the nanoribbons synthesized from elements where the thicknesses of $NbSe_3$ samples were from 20-30 nm to 95 nm.[24, 26] We do not rule out other possibilities for crystal fragmentation. Due to the crystal morphology of NbS_3 and $NbSe_3$, it is possible that they are cut during sonication similarly to carbon nanotubes or polymers.[54, 55] In that case cavitation bubbles induce high strain rates in the solvent and stretch the polymer eventually breaking chemical bonds. Sonication parameters such as time, power, frequency and device type may influence the nature of the forming nanostructures. Future studies should be able to identify appropriate conditions for predominant exfoliation of layers instead of cutting into 1D chains and chain scission. Also, separation methods such as gradient centrifugation may be useful for obtaining more homogenous samples.

Preparation and characterization of NbS_3 films

It is well known that multilayered films constructed of reassembled nanosheets of graphene or its inorganic analogues can have improved properties in the areas of supercapacitors, batteries, photoconductive materials, new magnetic materials etc.[9] We therefore further demonstrate applicability of our NbQ_3 colloid solutions to form thin films and investigate their properties.

NbS_3 films were prepared by two methods: (i) filtration of colloidal dispersions through 0.02 μm membrane filter "Whatman Anodisc"; and (ii) spraying colloidal dispersions on heated substrates (~ 200–250°C). The latter method is more flexible as it allows to prepare coatings of different complex configurations. Typical view of the films (Fig. 4 a and Figs. S8, S9 in the ESI) shows that thin films are quite smooth and transparent. The films were studied by powder X-ray diffraction (PXRD), Raman and IR spectroscopies.

As may be seen from PXRD data, films are characterized by strongly textured nature (Fig. 4 b). This fact may be expected from general structural consideration, but experimental evidence of such oriented packing is important. PXRD powder patterns of the films have high intensity of *00l* Bragg reflections. Figure S10 (ESI) compares calculated NbS_3 PXRD patterns for the samples with different degree of texture. Powder patterns were simulated by PowderCell 2.4 software[56] using cell parameters and atomic coordinates of single crystal NbS_3 data taken from Inorganic Crystal Structure Database, No. 2380. For simulation of textured X-Ray diffraction patterns we used Pseudo Voigt-2 profile

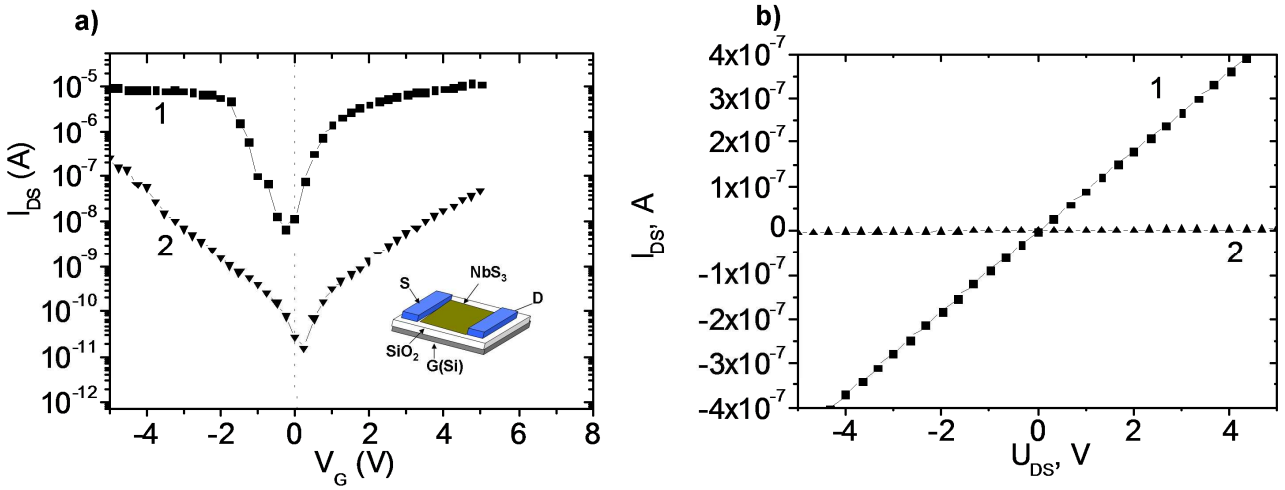

Fig. 5. a) I_{DS} (V_G) characteristics for NbS_3 films obtained from an ethanol/water colloid solution (1) and CH_3CN colloid solution (2). Drain-source voltage V_{DS} was 0.5 V. Inset shows device configuration; b) I_{DS} (V_{DS}) characteristics for the same NbS_3 films.

functions and the model of Rietveld-Toraya for plate crystals in Bragg-Brentano diffractometer geometry along *00l* directions with empirical coefficients O_1 which were changed and marked in Fig. S10 (ESI), and O_2 which was fixed to be 0. The texture coefficients were determined according to Eq. (1):

$$O_{HKL} = \sum_{i=1}^{MU} (o_1 + (1-o_1)e^{-o_2^2\phi^2}) \cdot \frac{\sum_j^S MU_j}{\sum_j^S O_j} \quad (1)$$

One can see that the increased O_1 parameter is responsible for texture. The intensities of Bragg reflections with indexes *00l* and *10l* increase, while intensities of other Bragg reflections (in normalized presentation) rapidly decrease and become negligible after O_1 exceeds 10. We can assume that powder patterns of NbS_3 films correspond to simulation with O_1 close to 20. These data show that nanosized particles of layered trichalcogenides are highly oriented in the film along *00l* planes indicating that during filtration they fall on the filter (and each other) in a similar manner.

Raman spectra of bulk and film NbS_3 samples recorded at λ = 488.0 nm are in good accordance with published data with only minor differences of peak positions.[57] Raman peaks in the two Raman spectra (Fig. 4 c) were assigned following previous work by Sourisseau et al.[57] Low-frequency peak at 151 cm^{-1} is caused by lattice compression along the columns ((T'_y) mode), and the one at 159 cm^{-1} is a Nb–Nb stretching mode. The prominent peak at 193 cm^{-1} may be assigned to υ(Nb–$(S_2)^{2-}$). Symmetrical valence Nb–S vibrations («rigid»-sublattice) appear at 260 cm^{-1}. Weak peaks in the area of 298–319 cm^{-1} may be ascribed to υ(Nb–S^{2-}) intrachain vibration, and the peaks at 375 cm^{-1} and 387 cm^{-1} originate from υ(Nb–S^{2-}) interchain modes. The high-frequency bands at 556–568 cm^{-1} are due to stretching vibrations of S–S bonds in $(S_2)^{2-}$ pairs. IR spectra also agree well with reported data (Fig. S11 in the ESI).[57] Therefore, XRD, IR and Raman spectroscopies confirm phase composition of the films: they are composed of well-crystallized triclinic NbS_3 nanoribbons, which are highly oriented in the film along *00l* planes.

Electrical properties of thin films

NbS_3 is a semiconductor with E_g of about 0.3 eV.[38, 40] As an example of the properties of the fabricated thin films we further study their current-voltage characteristics. Thin NbS_3 film (~ 0.5 – 1 μm) was deposited from colloidal dispersion by spray technology on a SiO_2/Si substrate in transistor configuration with the use of Si substrate as a gate (Fig. 5 a, inset). Two planar contacts (a drain and a source) were attached to NbS_3 layer on the SiO_2 surface, and the third contact was connected to the silicon substrate. The drain current I_{DS} as a function of V_{DS} was linear and demonstrated ohmic behavior of contacts attached to NbS_3 (Fig. 5 b). Taking into account the geometrical size of the samples, their sheet resistivities were $3.5 \cdot 10^6$ Ohm·sq^{-1} (1) and $1.3 \cdot 10^8$ Ohm·sq^{-1} (2). Measurement of current in the NbS_3 film as a function of gate voltage V_G allowed to calculate carrier mobility. The constant voltage applied between the drain and source ranged from 0.2 V to 1 V, and the dependence of the drain current on the gate voltage I_{DS} (V_G) was studied. From the I_{DS} (V_G) characteristics (Fig. 5), the ratio of the current of open channel I_{on} to the current of closed channel I_{off} and the value of the carrier mobility were calculated using traditional approach for semiconductor field-effect transistors. The electron (μ_e) and hole (μ_h) mobilities were determined from the linear slope of the I_{DS} (V_G) according to Eq. (2):

$$\mu = \frac{L}{C_{ox} W V_{DS}} \frac{\Delta I_{DS}}{\Delta V_g} \quad (2)$$

where μ is the carrier mobility, W and L are NbS_3 layer width and length, respectively, $C_{ox} = \varepsilon_{ox}\varepsilon_o/t_{ox}$ is the gate oxide capacitance (ε_{ox} = 3.9 is the dielectric constant of silicon dioxide and t_{ox} = 300 nm is the thickness of the gate oxide layer), and ΔI_{DS} is the shift of current I_{DS} induced by a gate-voltage change ΔV_g.

The highest carrier mobility was found in the NbS_3 films obtained from an ethanol/water colloid solution. In this case the mobility of electrons and holes was estimated as ~ 1200 – 2400 $cm^2V^{-1}s^{-1}$. The I_{DS} current value in the layer is modulated by the

gate voltage on the 3-4 orders of magnitude. For the NbS_3 layers, created from NbS_3/CH_3CN colloid solutions, carrier mobility determined from the similar I_{DS} (V_G) characteristics had values of ~10 $cm^2/V^{-1}s^{-1}$. Carrier mobility for films created from other solutions was even lower. The high value of carrier mobility for NbS_3/ethanol/water solution is most likely due to functionalization of the NbS_3 flakes by solvent molecules. The shift of Dirac (neutrality) point from zero to positive voltage for the film obtained from NbS_3/CH_3CN colloid solution corresponds to *p*-type doping, whereas Dirac point shift to negative voltage for the film obtained from NbS_3/ethanol/water solution corresponds to *n*-type conductivity. Change in doping type also may support a suggestion of functionalization of the NbS_3 flakes.

Conclusions

In conclusion, we have demonstrated for the first time that NbS_3 and $NbSe_3$ may be directly dispersed in low-boiling point organic solvents such as ethanol/water mixture or acetonitrile by sonication. Stable concentrated colloidal dispersions contain thin crystalline nanoribbons of transition metal trichalcogenides. They may be reassembled into well-textured thin films with good conducting properties. Our findings may be potentially extended to the whole family of transition metal trichalcogenides, and indeed our preliminary studies confirm that TiS_3, TaS_3, $NbSe_3$ may be exfoliated in this way as well. Solution processability of transition metal trichalcogenides opens up many opportunities for their use in thin film devices, batteries, supercapacitors, hybrids with other layered nanomaterials, polymer fillers and other applications yet to be discovered.

Experimental

The syntheses of niobium trichalcogenides were carried out using high temperature ampoule method starting from high purity elements (see ESI for more information).

Dispersions of NbS_3 and $NbSe_3$

Bulk powdered samples of NbS_3 (0.5 g) or $NbSe_3$ (0.8 g) were sonicated (Elmasonic S40 ultrasonic bath, ultrasound power 120 W) in 250 mL of a solvent (DMF, acetone, acetonitrile, water, ethanol, water-ethanol mixture (55/45 vol.%), isopropanol or *N*-methyl-2-pyrrolidone) for 30 hours. This resulted in brown-beige (NbS_3) or dark-grey ($NbSe_3$) non-transparent mixtures. The resulting mixtures were centrifuged at 2600 rpm for 30 minutes to remove large (heavy) particles.

Thin films

NbS_3 and $NbSe_3$ thin films were prepared from colloidal dispersions by their filtration using membrane filters Whatman Anodisc with pore size of 0.02 μm and by spray method. Film thickness may be varied according to the volume used. The thicknesses of the film prepared by filtration were from 0.25 to 9 μm, and the sprayed films were 0.5 – 1.0 μm thick.

Characterization

Powder X-Ray diffraction patterns of the synthesized compounds (both powder samples and films) were recorded using Philips PW1820/1710 X-Ray diffractometer (Cu Kα radiation, graphite monochromator, silicon plate used as an external standard). Raman spectra were excited with the 488.0 nm lines of an argon ion laser and analyzed with a Triplemate instrument. The particle size distribution for dispersions was estimated by dynamic light scattering (DLS) method using 90Plus Brookhaven Inst. UV-*vis* spectra of the dispersions were obtained using Ultrospec 3300 pro spectrometer in the wavelength interval of 200 – 1100 nm. HRTEM images were obtained on a JEM-2200FS electron microscope (JEOL, Japan) with a lattice-fringe resolution of 0.1 nm at an accelerating voltage of 200 kV. The high-resolution images of periodic structures were analyzed by the Fourier method. Samples to be examined by HRTEM were prepared on a perforated carbon film mounted on a copper grid. The thickness and surface morphology of particles were measured by scanning probe microscope (Solver P-47H, NT-MDT, Russia). Images were obtained in atomic force microscopy mode with using of non-contact cantilevers (NSG-11, NT-MDT, Russia).

Acknowledgements

The study was financially supported by Samsung Advanced Institute of Technology, Suwon, Korea (GRO Project) and by Siberian Branch of Russian Academy of Sciences (Project 75).

Notes and references

[a] *Nikolaev Institute of Inorganic Chemistry, Siberian Branch of the Russian Academy of Sciences, 3, Acad. Lavrentiev prospect, Novosibirsk, 630090, Russian Federation. Fax: +7383-330-94-89; Tel: +7383-330-92-53; E-mail: fed@niic.nsc.ru*
[b] *Novosibirsk State University, 2, Pirogova st., Novosibirsk, 630090, Russian Federation*
[c] *Rzhanov Institute of Semiconductor Physics, Siberian Branch of the Russian Academy of Sciences 13, Acad. Lavrentiev prospect, Novosibirsk, 630090, Russian Federation*
[d] *Samsung Advanced Institute of Technology, Suwon, South Korea*

† Electronic Supplementary Information (ESI) available: additional synthetic and characterization details (DLS, TEM, AFM, XRD, IR, photographs). See DOI: 10.1039/b000000x/

1. J. N. Coleman, M. Lotya, A. O'Neill, S. D. Bergin, P. J. King, U. Khan, K. Young, A. Gaucher, S. De, R. J. Smith, I. V. Shvets, S. K. Arora, G. Stanton, H.-Y. Kim, K. Lee, G. T. Kim, G. S. Duesberg, T. Hallam, J. J. Boland, J. J. Wang, J. F. Donegan, J. C. Grunlan, G. Moriarty, A. Shmeliov, R. J. Nicholls, J. M. Perkins, E. M. Grieveson, K. Theuwissen, D. W. McComb, P. D. Nellist and V. Nicolosi, *Science*, 2011, **331**, 568-571.
2. Z. Zeng, Z. Yin, X. Huang, H. Li, Q. He, G. Lu, F. Boey and H. Zhang, *Angew. Chem., Int. Ed.*, 2011, **50**, 11093-11097.
3. Y. Yao, Z. Lin, Z. Li, X. Song, K.-S. Moon and C.-p. Wong, *J. Mater. Chem.*, 2012, **22**, 13494-13499.
4. L. Ren, X. Qi, Y. Liu, G. Hao, Z. Huang, X. Zou, L. Yang, J. Li and J. Zhong, *J. Mater. Chem.*, 2012, **22**, 4921-4926.
5. Y. Du, Z. Yin, J. Zhu, X. Huang, X.-J. Wu, Z. Zeng, Q. Yan and H. Zhang, *Nat Commun*, 2012, **3**, 1177.
6. Z. Zeng, T. Sun, J. Zhu, X. Huang, Z. Yin, G. Lu, Z. Fan, Q. Yan, H. H. Hng and H. Zhang, *Angew. Chem., Int. Ed.*, 2012, **51**, 9052-9056.
7. V. Nicolosi, M. Chhowalla, M. G. Kanatzidis, M. S. Strano and J. N. Coleman, *Science*, 2013, **340**, 1226419.

8. K. J. Koski and Y. Cui, *ACS Nano*, 2013, **7**, 3739-3743.
9. S. Z. Butler, S. M. Hollen, L. Cao, Y. Cui, J. A. Gupta, H. R. Gutiérrez, T. F. Heinz, S. S. Hong, J. Huang, A. F. Ismach, E. Johnston-Halperin, M. Kuno, V. V. Plashnitsa, R. D. Robinson, R. S. Ruoff, S. Salahuddin, J. Shan, L. Shi, M. G. Spencer, M. Terrones, W. Windl and J. E. Goldberger, *ACS Nano*, 2013, **7**, 2898-2926.
10. M. Chhowalla, H. S. Shin, G. Eda, L.-J. Li, K. P. Loh and H. Zhang, *Nature Chem.*, 2013, **5**, 263-275.
11. S. Balendhran, S. Walia, H. Nili, J. Z. Ou, S. Zhuiykov, R. B. Kaner, S. Sriram, M. Bhaskaran and K. Kalantar-zadeh, *Adv. Funct. Mater.*, 2013, **23**, 3952–3970.
12. X. Huang, Z. Zeng and H. Zhang, *Chem. Soc. Rev.*, 2013, **42**, 1934-1946.
13. X. Song, J. Hu and H. Zeng, *J. Mater. Chem. C*, 2013, **1**, 2952-2969.
14. C. N. R. Rao, H. S. S. Ramakrishna Matte and U. Maitra, *Angew. Chem., Int. Ed.*, 2013, **52**, 13162-13185.
15. Z. Zeng, C. Tan, X. Huang, S. Bao and H. Zhang, *Energy Environ. Sci.*, 2014, **7**, 797-803.
16. J. Zheng, H. Zhang, S. Dong, Y. Liu, C. Tai Nai, H. Suk Shin, H. Young Jeong, B. Liu and K. Ping Loh, *Nat Commun*, 2014, **5**, 2995.
17. J. L. Gunjakar, I. Y. Kim, J. M. Lee, Y. K. Jo and S.-J. Hwang, *J. Phys. Chem. C*, 2014, **118**, 3847-3863.
18. S. K. Srivastava and B. N. Avasthi, *J. Mater. Sci.*, 1992, **27**, 3693-3705.
19. V. Y. Pokrovskii, S. G. Zybtsev, M. V. Nikitin, I. G. Gorlova, V. F. Nasretdinova and S. V. Zaitsev-Zotov, *Phys. Usp.*, 2013, **56**, 29-48.
20. H. Tang, C. Li, X. Yang, C. Mo, K. Cao and F. Yan, *Cryst. Res. Technol.*, 2011, **46**, 400-404.
21. D. W. Murphy and F. A. Trumbore, *J. Cryst. Growth*, 1977, **39**, 185-199.
22. Y. Ōnuki, R. Inada, S. Tanuma, S. Yamanaka and H. Kamimura, *Solid State Ionics*, 1983, **11**, 195-201.
23. S. Jeong, D. Yoo, J.-t. Jang, M. Kim and J. Cheon, *J. Am. Chem. Soc.*, 2012, **134**, 18233-18236.
24. Y. S. Hor, Z. L. Xiao, U. Welp, Y. Ito, J. F. Mitchell, R. E. Cook, W. K. Kwok and G. W. Crabtree, *Nano Lett.*, 2005, **5**, 397-401.
25. S. De, C. S. Boland, P. J. King, S. Sorel, M. Lotya, U. Patel, Z. L. Xiao and J. N. Coleman, *Nanotechnology*, 2011, **22**, 285202.
26. A. A. Stabile, L. Whittaker, T. L. Wu, P. Marley, M., S. Banerjee and G. Sambandamurthy, *Nanotechnology*, 2011, **22**, 485201.
27. E. Slot, M. A. Holst, H. S. J. van der Zant and S. V. Zaitsev-Zotov, *Phys. Rev. Lett.*, 2004, **93**, 176602.
28. M. O. King, M. Popland, S. J. Denholme, D. H. Gregory, D. A. MacLaren and M. Kadodwala, *Nanoscale*, 2012, **4**, 607-612.
29. H. Jin, D. Cheng, J. Li, X. Cao, B. Li, X. Wang, X. Liu and X. Zhao, *Solid State Sci.*, 2011, **13**, 1166-1171.
30. J. Ma, X. Liu, X. Cao, S. Feng and M. E. Fleet, *Eur. J. Inorg. Chem.*, 2006, **2006**, 519-522.
31. F. A. Trumbore and L. W. Ter Haar, *Chem. Mater.*, 1989, **1**, 490-492.
32. T. Matsuura, S. Tanda, K. Asada, Y. Sakai, T. Tsuneta, K. Inagaki and K. Yamaya, *Physica B: Condensed Matter*, 2003, **329–333, Part 2**, 1550-1551.
33. S. Tanda, T. Tsuneta, Y. Okajima, K. Inagaki, K. Yamaya and N. Hatakenaka, *Nature*, 2002, **417**, 397-398.
34. A. N. Enyashin and A. L. Ivanovskiĭ, *Phys. Solid State*, 2006, **48**, 780-785.
35. A. Grisel, F. Lévy and T. J. Wieting, *Physica B+C*, 1980, **99**, 365-370.
36. S. P. Gwet, Y. Mathey and C. Sourisseau, *Phys. Status Solidi B*, 1984, **123**, 503-517.
37. K. R. Zhdanov, A. V. Mishenko, F. S. Rakhmenkulov and V. E. Fedorov, *physica status solidi (a)*, 1984, **83**, 147-152.
38. L. A. Grigoryan and A. V. Novoselova, *Dokl. Chem.*, 1962, **144**, 795-797.
39. J. Rijnsdorp and F. Jellinek, *J. Solid State Chem.*, 1978, **25**, 325-328.
40. M. E. Itkis, F. Y. Nad, S. V. Zaitsevzotov and F. Levy, *Solid State Commun.*, 1989, **71**, 895-898.
41. P. Monceau, N. P. Ong, A. M. Portis, A. Meerschaut and J. Rouxel, *Phys. Rev. Lett.*, 1976, **37**, 602-606.
42. J. Chaussy, P. Haen, J. C. Lasjaunias, P. Monceau, G. Waysand, A. Waintal, A. Meerschaut, P. Molinie and J. Rouxel, *Solid State Commun.*, 1976, **20**, 759-763.
43. T. Sambongi, K. Tsutsumi, Y. Shiozaki, M. Yamamoto, K. Yamaya and Y. Abe, *Solid State Commun.*, 1977, **22**, 729-731.
44. C. Roucau, R. Ayroles, P. Monceau, L. Guemas, A. Meerschaut and J. Rouxel, *Phys. Status Solidi A-Appl. Res.*, 1980, **62**, 483-493.
45. T. Sambongi, M. Yamamoto, K. Tsutsumi, Y. Shiozaki, K. Yamaya and Y. Abe, *J. Phys. Soc. Jpn.*, 1977, **42**, 1421-1422.
46. P. Haen, F. Lapierre, P. Monceau, M. Nunez Regueiro and J. Richard, *Solid State Commun.*, 1978, **26**, 725-730.
47. M. Yamamoto, *J. Phys. Soc. Jpn.*, 1978, **45**, 431-438.
48. R. R. Chianelli and M. B. Dines, *Inorg. Chem.*, 1975, **14**, 2417-2421.
49. M. Zanini, *J. Electrochem. Soc.*, 1985, **132**, 588-593.
50. K. Yamaya, T. H. Geballe, J. V. Acrivos and J. Code, *Physica B+C*, 1981, **105**, 444-447.
51. K. Inagaki, T. Toshima, S. Tanda, K. Yamaya and S. Uji, *Appl. Phys. Lett.*, 2005, **86**, 073101.
52. Q. Xiang, J. Yu and M. Jaroniec, *J. Am. Chem. Soc.*, 2012, **134**, 6575-6578.
53. K.-G. Zhou, N.-N. Mao, H.-X. Wang, Y. Peng and H.-L. Zhang, *Angew. Chem., Int. Ed.*, 2011, **50**, 10839-10842.
54. F. Hennrich, R. Krupke, K. Arnold, J. A. Rojas Stütz, S. Lebedkin, T. Koch, T. Schimmel and M. M. Kappes, *J. Phys. Chem. B*, 2007, **111**, 1932-1937.
55. G. Pagani, M. J. Green, P. Poulin and M. Pasquali, *Proceedings of the National Academy of Sciences*, 2012, **109**, 11599-11604.
56. , W. Kraus, G. Nolze, PowderCell 2.4, Program for the Representation and Manipulation of Crystal Structures and Calculation of the Resulting X-Ray Powder Patterns, Berlin, 2000.
57. C. Sourisseau, R. Cavagnat, M. Fouassier and P. Maraval, *J. Raman Spectrosc.*, 1990, **21**, 337-349.

Liquid-phase exfoliation of niobium trisulfide and niobium triselenide

Vladimir E. Fedorov,*[a, b] Sofya B. Artemkina,[a,b] Ekaterina D. Grayfer,[a] Nikolay G. Naumov,[a,b] Yuri V. Mironov,[a] Alexander I. Bulavchenko,[a] Vladimir I. Zaikovskii,[b] Irina V. Antonova,[c] Alexander I. Komonov,[c] and Maxim V. Medvedev[d]

[a]Nikolaev Institute of Inorganic Chemistry, Siberian Branch of Russian Academy of Sciences, 3, Acad. Lavrentiev prospect, Novosibirsk, 630090, Russian Federation

[b]Novosibirsk State University, 2, Pirogova street, Novosibirsk, 630090, Russian Federation

[c]Rzhanov Institute of Semiconductor Physics, Siberian Branch of Russian Academy of Sciences, 13, Acad. Lavrentiev prospect, Novosibirsk, 630090, Russian Federation

[d]Samsung Advanced Institute of Technology, Suwon, South Korea

*Corresponding author. Tel. +7383-330-92-53; E-mail: fed@niic.nsc.ru

Table of contents entry

Bulk niobium trichalcogenides NbS_3 and $NbSe_3$ were stably dispersed in a number of common organic solvents by ultrasonic treatment to yield colloids containing thin well-crystallized nanoribbons of NbS_3 and $NbSe_3$.